Mustafa Turkyilmazoglu*

# Magnetic Field and Slip Effects on the Flow and Heat Transfer of Stagnation Point Jeffrey Fluid over Deformable Surfaces

DOI 10.1515/zna-2016-0047
Received January 14, 2016; accepted April 13, 2016; previously published online May 9, 2016

**Abstract:** The Mhd slip flow and heat transfer of stagnation point Jeffrey fluid over deformable surfaces are the state of the art of this article. Following an analytical approach, the existence, uniqueness, and possible multiplicity of the physical solutions affected by several physical parameters are investigated. Particularly, magnetic interaction and slip factor are shown to much influence the structure of the solutions regarding both momentum and thermal boundary layers. The presented exact solutions not only provide a clear understanding of fruitful physical mechanisms present in this nonlinear flow problem but they have also merits in calculations by means of numerous numerical schemes aiming to explore further complex phenomena.

**Keywords:** Analytical Solutions; Deformable Sheets; Jeffrey Stagnation Point Fluid; Magnetohydrodynamic Flow; Slip Velocity.

## 1 Introduction

The engineering processes during the manufacture of certain materials such as insulating appliances and paper production involve the fluid flow and heat developing over deformable surfaces (sheets) [1]. The present analytical work is hence devoted to the momentum and thermal boundary layer flow over such surfaces taking into account of potential Mhd and slip effects.

The importance of physical phenomena on deformable surfaces attracted many scientists, see for instance the analytical results in the publications [2–5]. Since the convected derivatives are substituted with the time derivatives, the linear model of Jeffrey fluid is preferred in many applications [6]. The significance of Mhd effects and other physical mechanisms was emphasised in many Jeffrey fluid flow applications. To date, analytical solutions for the flow of a Jeffrey fluid over a shrinking sheet were described in [7]. The Jeffrey fluid model for the peristaltic flow of chyme in the small intestine was given in [8]. The Jeffrey fluid flow in tubes of small diameters was studied in [9]. The unsteady oscillatory stagnation point flow of a Jeffrey fluid was examined in [10]. The MHD flow of Jeffrey fluid over a stretching cylinder was analysed in [11]. An analysis of the boundary layer flow and heat transfer in a Jeffrey fluid containing nanoparticles was presented in [12]. Further interesting physical features of stretching surfaces were explored in the articles [13–15].

Although stagnation-point flows are difficult to examine analytically, and hence much work is diverted to numerical means, a successful analytical work was fulfilled in [16]. Exact solutions of the exponential or linear forms were presented in the latter involving many physical parameters.

The motivation of this article is to extend the article [16] to cover the effects of Mhd and slip in a Jeffrey stagnation point fluid flow forming over deformable sheets. These effects are thought to be important in engineering applications. It is indeed found that the obtained analytical solutions are considerably influenced by such physical mechanisms.

## 2 Mathematical Formulation

The Jeffrey fluid flow considered in this work is the laminar steady state developing along the $x$-axis near the stagnation point of a permeable stretching/shrinking surface lying at $y=0$, see Figure 1. The deforming velocity of the wall is $u_w(x)$, at which a uniform external magnetic field of strength $B_0$ is applied. At the far field, a uniform ambient temperature $T_\infty$ is assumed together with a potential flow $u_e(x)$. The equations of flow and temperature are then stated as

***Corresponding author: Mustafa Turkyilmazoglu,** Department of Mathematics, Hacettepe University, 06532-Beytepe, Ankara, Turkey, E-mail: turkyilm@hotmail.com

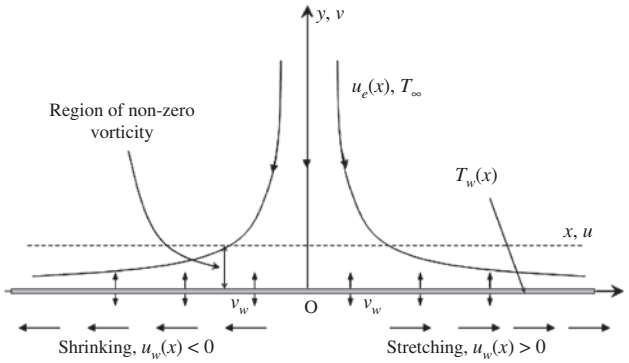


**Figure 1:** The flow configuration.

$$\begin{aligned} &u_x+v_y=0,\\ &uu_x+vu_y=u_eu_{ex}+\frac{\nu}{1+\gamma_1}[u_{yy}+\gamma_2(uu_{xyy}-u_xu_{yy}+u_yu_{xy}+vu_{yyy})]\\ &\qquad -\sigma B_0^2(u-u_e),\\ &uT_x+vT_y=\alpha T_{yy}, \end{aligned} \tag{1}$$

with the boundary conditions

$$\begin{aligned} &u=dcx+lu',\ \ v=v_w,\ \ T=T_w(x)\ \ \text{at}\ \ y=0,\\ &u\to u_e(x)=ax,\ \ u_y\to 0,\ \ T\to T_\infty\ \ \text{as}\ \ y\to\infty. \end{aligned} \tag{2}$$

It is noted that the wall temperature $T_w(x)$ is either constant $T_w$ or evolving with $x$ linearly via $T_w(x)=T_w+bx$. $u$ and $v$ represent components of velocity in the $x$ and $y$ directions, $l$ is the slip constant depending on $\gamma_1$, refer to [17–19], and $v_w$ is the mass flux (for suction $v_w<0$ and for injection $v_w>0$). The temperature of the fluid is $T$, the thermal diffusivity is $\alpha$, the kinematic viscosity is $\nu$, and the electrical conductivity is $\sigma$. We should note that the fluid properties are assumed to be constant, for the purpose of gaining exact solutions. Otherwise, numerical means may be required [20]. Further, $\gamma_1$ and $\gamma_2$ are related to relaxation parameters. Finally, the stretching means $d=1$ and the shrinking means is $d=-1$, see [16].

## 3 Analytical Solutions

The following convenient transformations

$$\begin{aligned} &\eta=y\sqrt{\frac{c(1+\gamma_1)}{\nu}},\ \ u=cxf'(\eta),\ \ v=-\sqrt{\frac{c\nu}{1+\gamma_1}}f(\eta),\\ &\theta=\frac{T-T_\infty}{T_w-T_\infty}, \end{aligned} \tag{3}$$

are made use in a goal of obtaining similarity solutions form (1–2) which are reduced to

$$\begin{aligned} &f'''+ff''-f'^2+\beta(f''^2-ff^{(4)})+\Lambda^2-M(f'-\Lambda)=0,\\ &\theta''+Prf\theta'=0,\ \ (\text{for}\ \ T_w(x)=T_w),\\ &\theta''+Pr(f\theta'-f'\theta)=0,\ \ (\text{for}\ \ T_w(x)=T_w+bx) \end{aligned} \tag{4}$$

accompanied with the transformed boundary constraints

$$\begin{aligned} &f(0)=s,\ \ f'(0)=d+Lf''(0),\ \ \theta(0)=1\\ &f'(\infty)=\Lambda,\ \ f''(\infty)=0,\ \ \theta(\infty)=0. \end{aligned} \tag{5}$$

Here, $v_w=-\sqrt{\frac{c\nu}{1+\gamma_1}}s$ is the wall transpiration, $L$ the slip parameter, $\mathrm{Pr}=\frac{\nu}{\alpha}$ the usual Prandtl number, $\beta=c\gamma_2$ the Deborah number, $s$ the wall permeability, and $\Lambda=\frac{a}{c}$ a stagnation parameter so-called as the strength parameter and $M$ is the magnetic interaction parameter. Thus, the parameters $\beta$, $s$, Pr, and $\Lambda$ are the dominating parameters of the Jeffrey fluid flow. We should address that (4) and (5) turn out to be the problem studied Nazar et al. [21] in the case of a regular fluid $\beta=0$ and $M=L=0$.

The practical parameters of concerns are the local Nusselt number $\mathrm{Nu}_x$ and the skin friction coefficient $C_f$, given as usual from the definition

$$C_f=\frac{\tau_w}{\rho u_e^2(x)},\ \ \mathrm{Nu}_x=\frac{xq_w}{\alpha(T_w-T_\infty)}$$

together with the wall shear ad heat flux

$$\tau_w=\mu u_y(y=0),\ \ q_w=-\alpha T_y(y=0).$$

Consequently, the skin friction and Nusselt number may be determined from $-f''(0)$, $-\theta'(0)$.

Our analysis is basically based on the Crane's solution [22]

$$f(\eta)=1-e^{-\eta},$$

in the simplest flow situation with $M=L=\Lambda=\beta=s=0$. Hence, for the general case, we may impose a solution of the form

$$f(\eta)=s+\Lambda\eta+\frac{d-\Lambda}{\lambda(1+L\lambda)}(1-e^{-\lambda\eta}), \tag{6}$$

which must come along with the constraint $\lambda>0$ to achieve physical solutions. On substitution of (6) into the first of (4), we obtain the algebraic formula relating the physical parameters

$$\begin{aligned} &(d-\Lambda)[d(-1+\beta\lambda^2)+(1+L\lambda)(-M+\lambda(-s+\lambda+s\beta\lambda^2))\\ &\qquad -\Lambda-2L\lambda\Lambda-\beta\lambda^2\Lambda+\eta\lambda\Lambda(1+L\lambda)(-1+\beta\lambda^2)]=0. \end{aligned} \tag{7}$$

So, the shape of the solutions and the number of them will be specified from the roots of the polynomial (7).

## 4 Results and Discussion

In the particular case of $\Lambda=0$, (7) becomes

$$d(-1+\beta\lambda^2)+(1+L\lambda)(-M+\lambda(-s+\lambda+s\beta\lambda^2))=0, \tag{8}$$

and hence the momentum and thermal solutions exactly match with those already appeared in Turkyilmazoglu [2, 5].

In the case of linear wall temperature, the exact form of (6) and the energy equation in (4) suggest that an additional solution may also be obtained assuming

$$\theta=e^{-\lambda\eta}, \tag{9}$$

that yields

$$d\,\mathrm{Pr}+(\mathrm{Pr}\,s-\lambda)\lambda(1+L\lambda)=0, \tag{10}$$

From (8) and (10), it is easy to get

$$\lambda=\sqrt{\frac{1-\mathrm{Pr}+\sqrt{(-1+\mathrm{Pr})^2+4M\,\mathrm{Pr}\,\beta}}{2\beta}},$$
$$s=\frac{\lambda}{\mathrm{Pr}}-\frac{d}{\lambda(1+L\lambda)}. \tag{11}$$

As a result, one obtains

$$f=s+d\frac{1-e^{-\lambda\eta}}{\lambda(1+L\lambda)},$$
$$\theta=e^{-\lambda\eta}, \tag{12}$$

Since $\lambda$ is independent from $d$ and $L$, temperature is not influenced by these parameters. However, the corresponding suction parameter $s$ will change with these parameter. The physically interesting parameters are then

$$-f''(0)=\frac{d\lambda}{1+L\lambda},\quad -\theta'(0)=\lambda.$$

Therefore, the skin friction coefficient will decrease by increasing slip parameter.

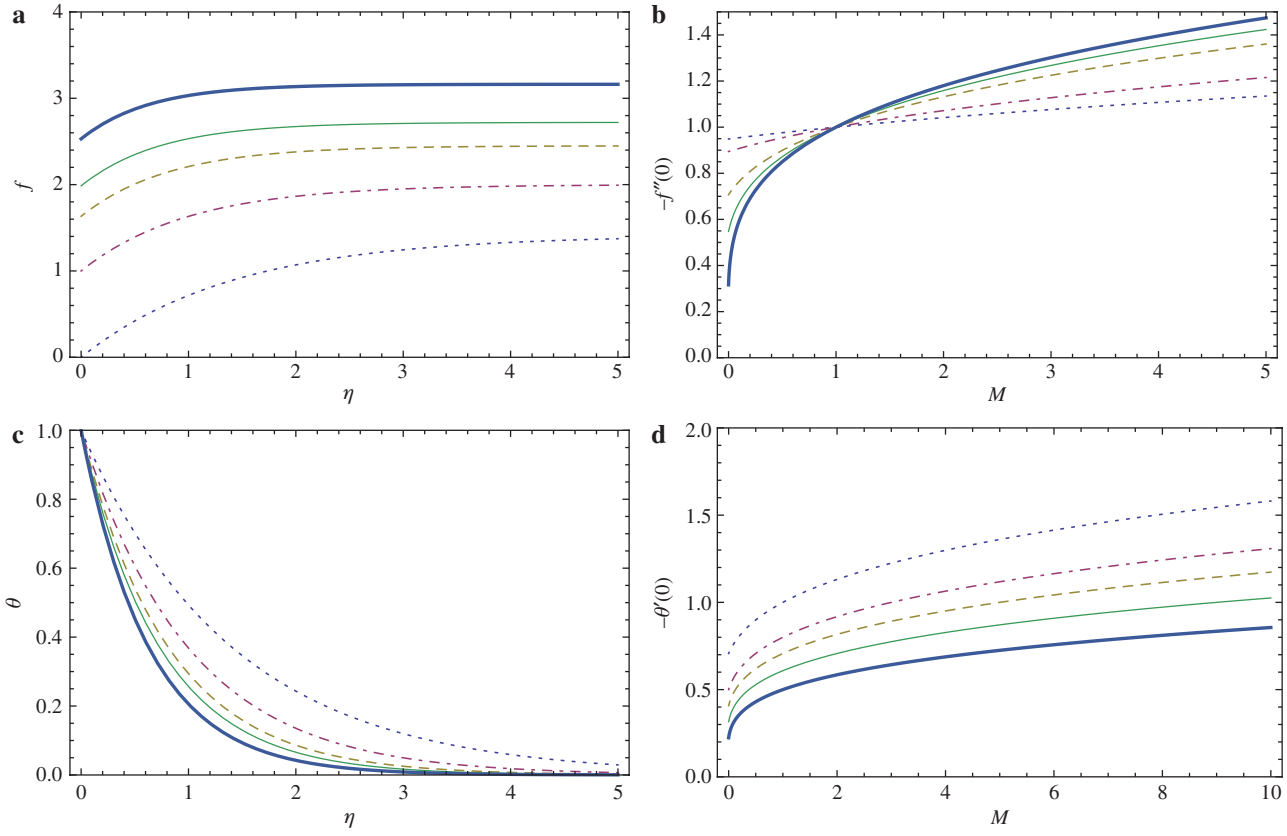


**Figure 2:** (a) ($f$) at $d=1$, $\mathrm{Pr}=1/2$, $L=0$, and $\beta=1$ (dotted, dot-dashed, dashed, thin, and thick curves are for $M=0$, 1, 3, 5, and 10, respectively); (b) $-f''(0)$ at $d=1$, $L=0$, and $\beta=1$ (curves for $\mathrm{Pr}=1/10$ dotted, $\mathrm{Pr}=2/10$ dot-dashed, $\mathrm{Pr}=5/10$ dashed, $\mathrm{Pr}=7/10$ thin, and $\mathrm{Pr}=9/10$ thick); (c) $\theta$ at $\mathrm{Pr}=1/2$ and $\beta=1$ (dotted, dot-dashed, dashed, thin, and thick curves are for $M=0$, 1, 3, 5, and 10, respectively); and (d) $-\theta'(0)$ at $\mathrm{Pr}=1/2$ (dotted, dot-dashed, dashed, thin, and thick curves are for $\beta=1$, 2, 3, 5, and 10, respectively).

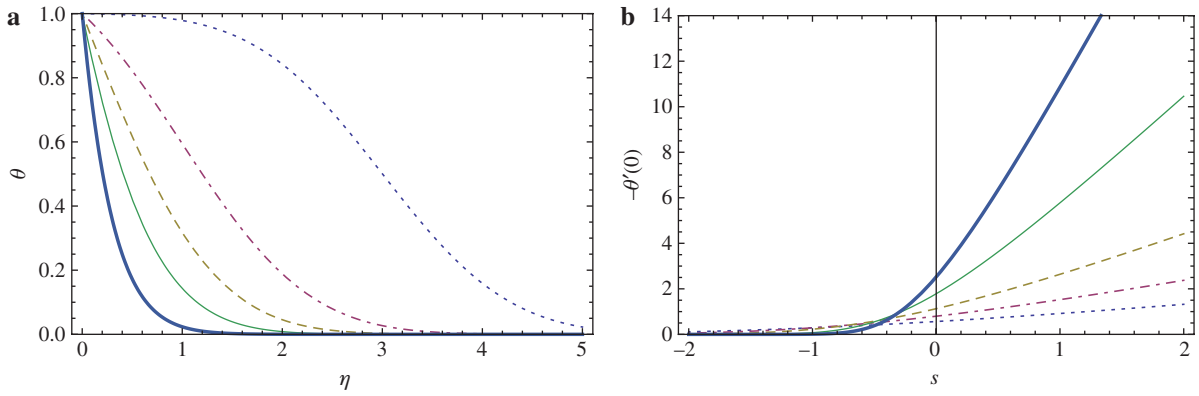


**Figure 3:** Temperature and heat transfer rate. (a) $\theta$ for Pr = 1 for varying $s$ (curves for $s = -3$ dotted, $s = -1$ dot-dashed, $s = 0$ dashed, $s = 1$ thin, and $s = 3$ thick) and (b) $-\theta'(0)$ for varying Pr (curves for Pr = 1/2 dotted, Pr = 1 dot-dashed, Pr = 2 dashed, Pr = 5 thin, and Pr = 10 thick).

**Table 1:** Variations of $-\theta'(0)$ for $\Lambda = d = 1$.

| Pr | $s=-5$ | $s=-1$ | $s=0$ | $s=1$ | $s=5$ |
|---|---|---|---|---|---|
| 1/2 | 0.00054468 | 0.28897818 | 0.56418958 | 0.91635282 | 2.67634038 |
| 1 | 0.00000149 | 0.28759997 | 0.79788456 | 1.52513528 | 5.18650397 |
| 2 | 0.00000000 | 0.22527124 | 1.12837917 | 2.63896751 | 10.1927001 |
| 5 | 0.00000000 | 0.07416485 | 1.78412412 | 5.77772456 | 25.1969210 |
| 10 | 0.00000000 | 0.00850703 | 2.52313252 | 10.8602968 | 50.1984311 |

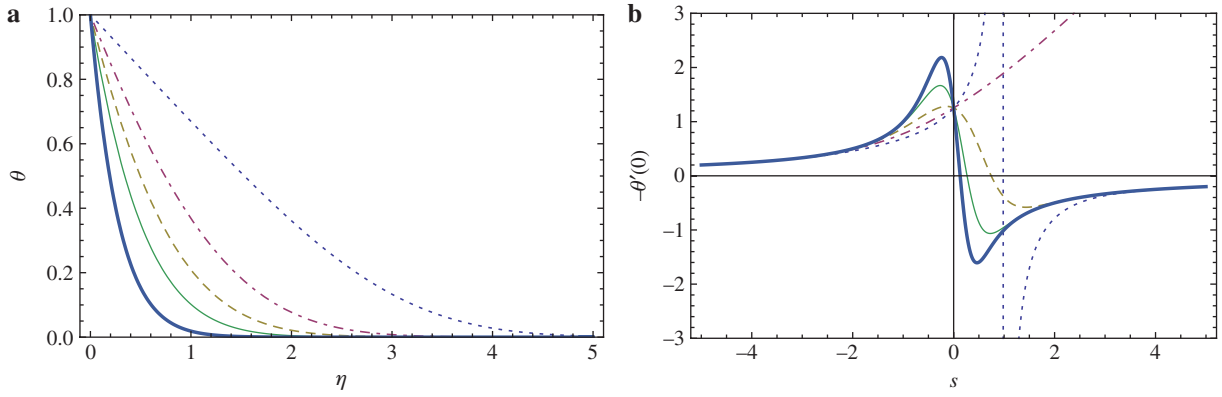


**Figure 4:** Temperature and heat transfer rate. (a) $\theta$ for Pr = 1 for varying $s$ (curves for $s = -3$ dotted, $s = -1$ dot-dashed, $s = 0$ dashed, $s = 1$ thin, and $s = 3$ thick) and (b) $-\theta'(0)$ for varying Pr (curves for Pr = 1/2 dotted, Pr = 1 dot-dashed, Pr = 2 dashed, Pr = 5 thin, and Pr = 10 thick).

The distributions of velocity and temperature and also variations of wall shear and Nusselt number, drawn from (12), are well captured in Figure 2a–d for a variety of magnetic interaction parameters $M$. As revealed in the figure, the magnetic field has much impact on the fields, by increasing $f$ and decreasing $\theta$. As a result, the thickness of boundary is enhanced as opposed to the thickness of thermal layer. This phenomenon is quite different from the usual influence of magnetic field, see Turkyilmazoglu [2, 5]. As a result, the range of parameters obtained in this section is of considerable significance in physics, since strong magnetic interaction yields higher skin friction and smaller heat transfer rate.

For the specific case of $\Lambda = 1$ as well as $d = 1$, the Jeffrey fluid will evolve to

$$f = s + \eta, \tag{13}$$

valid for any $M$, $L$, $s$, and $\beta$. Together, a temperature solution is also given by

$$\theta=\frac{Erfc\left[\frac{\sqrt{\Pr}(s+\eta)}{\sqrt{2}}\right]}{Erfc\left[\frac{\sqrt{\Pr}s}{\sqrt{2}}\right]}, \tag{14}$$

where *Erfc* means the complementary error function. Hence, we get the exact expression

$$-\theta'(0)=\frac{e^{-\frac{\Pr s^2}{2}}\sqrt{\frac{2}{\pi}}\sqrt{\Pr}}{Erfc\left[\frac{\sqrt{\Pr}s}{\sqrt{2}}\right]}. \tag{15}$$

The temperature and heat transfer rate can be visualised from Figure 3a and b together with Table 1.

An extra solution for the temperature may also be found as

$$\theta=\frac{e^{-\frac{1}{2}\Pr\eta(2s+\eta)}\left(2+e^{\frac{1}{2}\Pr(s+\eta)^2}\sqrt{2\pi}(s+\eta)\left(-1+\sqrt{\Pr}Erf\left[\frac{\sqrt{\Pr}(s+\eta)}{\sqrt{2}}\right]\right)\right)}{2+e^{\frac{\Pr s^2}{2}}\sqrt{2\pi}s\left(-1+\sqrt{\Pr}Erf\left[\frac{\sqrt{\Pr}s}{\sqrt{2}}\right]\right)}, \tag{16}$$

where *Erf* is the error function. The rate of heat transfer is later

$$-\theta'(0)=\frac{1}{-s+\frac{e^{-\frac{\Pr s^2}{2}}\sqrt{\frac{2}{\pi}}}{1-\sqrt{\Pr}Erf\left[\frac{\sqrt{\Pr}s}{\sqrt{2}}\right]}}. \tag{17}$$

Figure 4a and b together with Table 2 explains the physical mechanisms of Jeffrey fluid flow and heat.

It is also possible to get a simple solution of the form

$$f=s-\eta, \tag{18}$$

that is ture for all $s$ and $\beta$, when $\Lambda=-1$ and $d=-1$. Dissipation effects must be accounted for to get temperature solutions.

Eventually, if $\Lambda\neq 0$ we have from (7)

$$\beta=\frac{1}{M+2\Gamma}, \tag{19}$$

$$\lambda=\sqrt{M+2\Gamma}. \tag{20}$$

Thus, $f$ becomes

$$f=s+\Lambda\eta+\frac{(1-e^{-\eta\sqrt{M+2\Lambda}})(d-\Lambda)}{\sqrt{M+2\Lambda}(1+L\sqrt{M+2\Lambda})}, \tag{21}$$

leading to the skin friction

$$-f''(0)=\frac{(d-\Lambda)\sqrt{M+2\Lambda}}{1+L\sqrt{M+2\Lambda}}. \tag{22}$$

All these match with those given in [16] when $M=L=0$.

Figures 5a, b and 6a, b demonstrate the skin friction coefficient $-f''(0)$, for both the deforming sheets. Considerable decrease in the skin friction is exhibited by $\Lambda$. In addition, the skin friction is exhibited to increase to

$$L=\frac{d-M-3\Lambda}{(M+2\Lambda)^{3/2}},\quad -f''(0)=(M+2\Lambda)^{3/2},$$

which is the critical point from where a decrease commences for increasing $\Lambda$. The overall effect of magnetic field is to enhance the skin friction for the sheet with stretching and reduce it for the sheet with shrinking. Moreover, the slip parameter constantly decreases the skin friction as expected from (22).

Constant wall temperature solution is then

$$\theta=\frac{\phi(0)-\phi(\eta)}{\phi(0)}, \tag{23}$$

**Table 2:** Variations of $-\theta'(0)$ for $\Lambda=d=1$.

| Pr | $s=-5$ | $s=-1$ | $s=0$ | $s=1$ | $s=5$ |
|---|---|---|---|---|---|
| 1/2 | 0.19996391 | 0.68765459 | 1.25331414 | −59.855828 | −0.2002103 |
| 1 | 0.19999994 | 0.77663873 | 1.25331414 | 1.90427123 | 5.36181624 |
| 2 | 0.20000000 | 0.88189466 | 1.25331414 | −0.3951476 | −0.2000000 |
| 5 | 0.20000000 | 0.97981612 | 1.25331414 | −0.9473892 | −0.2000000 |
| 10 | 0.20000000 | 0.99870851 | 1.25331414 | −0.9975142 | −0.2000000 |

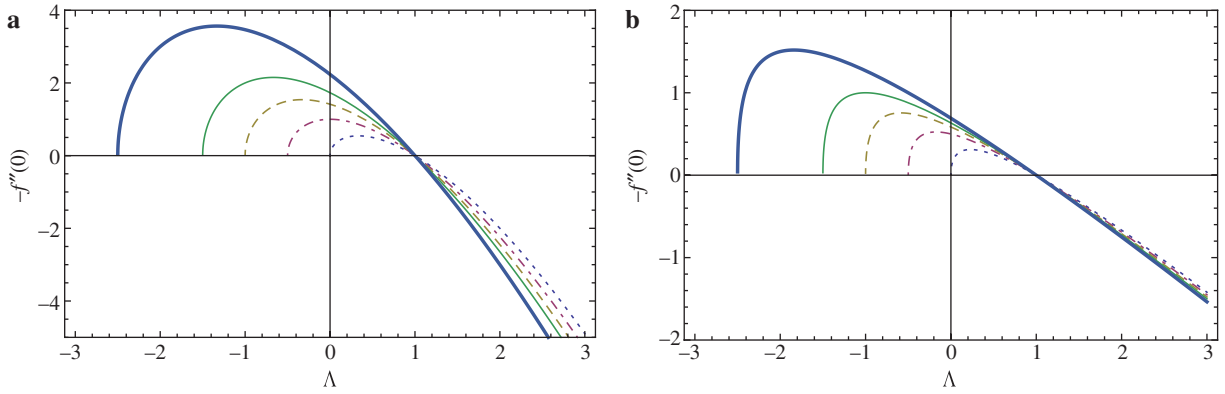


**Figure 5:** $-f''(0)$ for stretching sheet. (a) $L=0$ and (b) $L=1$. Dotted, dot-dashed, dashed, thin, and thick curves are for $M=0$, 1, 2, 3, and 5, respectively.

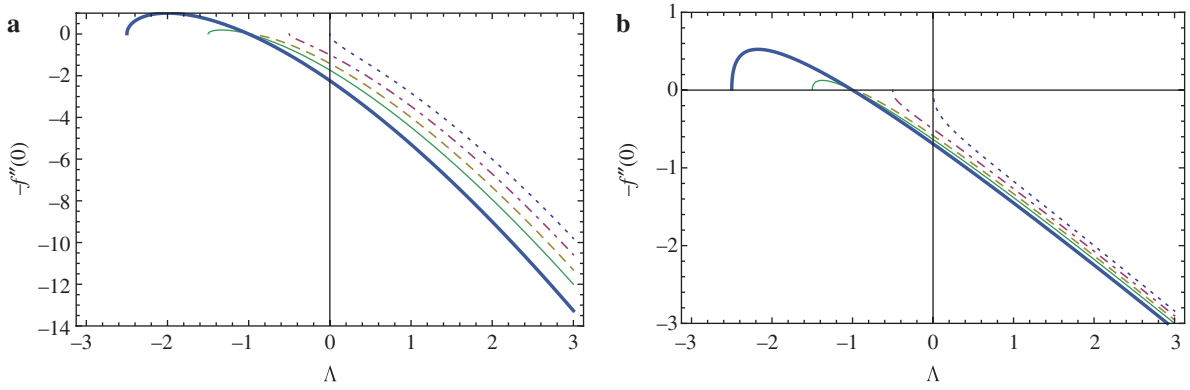


**Figure 6:** $-f''(0)$ for shrinking sheet. (a) $L=0$ and (b) $L=1$. Dotted, dot-dashed, dashed, thin, and thick curves are for $M=0$, 1, 2, 3, and 5, respectively.

**Table 3:** Variations of $-\theta'(0)$ when $M=L=s=0$.

| Pr | $\Lambda=1/2$ | $\Lambda=1$ | $\Lambda=2$ | $\Lambda=5$ | $\Lambda=10$ |
|---|---|---|---|---|---|
| 1/2 | 0.49038708 | 0.56418959 | 0.70450749 | 1.02506823 | 1.40783169 |
| 1 | 0.71543562 | 0.79788456 | 0.96926459 | 1.37894172 | 1.87737263 |
| 2 | 1.03915887 | 1.12837918 | 1.33240185 | 1.84715219 | 2.48819380 |
| 5 | 1.68862027 | 1.78412411 | 2.03141133 | 2.70930624 | 3.58685619 |
| 10 | 2.42444639 | 2.52313252 | 2.80151281 | 3.61951973 | 4.71703375 |

where $\phi(x)$ is given by

$$\int_0^x e^{-\frac{\Pr\left(\frac{e^{-x\sqrt{M+2\Lambda}}(d-\Lambda)}{\sqrt{M+2\Lambda}}+\frac{1}{2}x^2\Lambda\sqrt{M+2\Lambda}(1+L\sqrt{M+2\Lambda})+x(d-\Lambda+s\sqrt{M+2\Lambda}+Ls(M+2\Lambda))\right)}{\sqrt{M+2\Lambda}(1+L\sqrt{M+2\Lambda})}} dx.$$

Using (23), we obtain the Nusselt number

$$-\theta'(0)=\frac{e^{-\frac{\Pr(d-\Lambda)}{(M+2\Lambda)(1+L\sqrt{M+2\Lambda})}}}{\phi(0)}, \tag{24}$$

see Tables 3–6 for general insight.

We should emphasise that the heat transfer analysis is not restricted to the parameters as studied here, but it can be extended to the any desired real numbers, which may not be possible in numerical investigations.

## 5 Concluding Remarks

This article aims at extending the recent Jeffrey fluid flow and heat analysis carried out in [16] to incorporate the

**Table 4:** Variations of $-\theta'(0)$ when $M=L=s=0$.

| Pr | $\Lambda=1/2$ | $\Lambda=1$ | $\Lambda=2$ | $\Lambda=5$ | $\Lambda=10$ |
|---|---|---|---|---|---|
| 1/2 | 0.13265677 | 0.30301729 | 0.51837784 | 0.90709277 | 1.32438454 |
| 1 | 0.11231583 | 0.34568637 | 0.64507410 | 1.17313230 | 1.73176565 |
| 2 | 0.06597476 | 0.36252779 | 0.77787558 | 1.49425709 | 2.23844244 |
| 5 | 0.00872168 | 0.30420217 | 0.93153385 | 2.00564028 | 3.08852358 |
| 10 | 0.00019617 | 0.18229060 | 0.98643041 | 2.45016895 | 3.88829079 |

**Table 5:** Variations of $-\theta'(0)$ for $s=0$ and $M=L=1$.

| Pr | $\Lambda=1/2$ | $\Lambda=1$ | $\Lambda=2$ | $\Lambda=5$ | $\Lambda=10$ |
|---|---|---|---|---|---|
| 1/2 | 0.43017564 | 0.56418959 | 0.77091175 | 1.20844785 | 1.71791162 |
| 1 | 0.61832372 | 0.79788456 | 1.08225563 | 1.69377089 | 2.41079865 |
| 2 | 0.88846060 | 1.12837918 | 1.51936685 | 2.37420781 | 3.38359388 |
| 5 | 1.43128005 | 1.78412411 | 2.38096216 | 3.71384745 | 5.30138399 |
| 10 | 2.04769185 | 2.52313252 | 3.34770137 | 5.21582292 | 7.45360883 |

**Table 6:** Variations of $-\theta'(0)$ for $s=0$ and $M=L=1$.

| Pr | $\Lambda=1/2$ | $\Lambda=1$ | $\Lambda=2$ | $\Lambda=5$ | $\Lambda=10$ |
|---|---|---|---|---|---|
| 1/2 | 0.30602554 | 0.47872669 | 0.71687246 | 1.18183487 | 1.70317186 |
| 1 | 0.40007339 | 0.64926949 | 0.98911010 | 1.64826587 | 2.38569592 |
| 2 | 0.51485264 | 0.87693832 | 1.36331427 | 2.29866673 | 3.34211777 |
| 5 | 0.69985449 | 1.30030014 | 2.08493869 | 3.57243815 | 5.22427589 |
| 10 | 0.86287781 | 1.75132706 | 2.88092614 | 4.99512729 | 7.33390091 |

effects of Mhd and velocity slip occurring over deformable surfaces in the vicinity of stagnation point. For a regular fluid away from the stagnation point, exact or numerical solutions are available in the open literature. On the other hand, for stagnation point flow, the exact solutions are restricted to the publication [16]. Therefore, it is quite significant to cover the analytical extension of [16] in the presence of Mhd and slip velocity influences. For some particular parameter regimes, analytical solutions representing the momentum and thermal boundary layers concerning the stagnation Jeffrey fluid are presented, evolving into the solutions given in Turkyilmazoglu [2, 5] for further special restrictions. The results point to a range of parameters which are of quite importance in physics, since strong magnetic interaction yields higher skin friction and smaller heat transfer rate.

The intention here is to address the phenomenon of constant surface heating. However, the constant heat flux boundary condition may also warrant further work. Furthermore, the present analytic method may also be used for the dusty fluid and nanofluid models as appropriate for [23] and [24].

# References


[1] E. M. Sparrow and J. P. Abraham, Int. J. Heat Mass Transfer **48**, 3047 (2005).
[2] M. Turkyilmazoglu, J. Thermophys. Heat Transfer **25**, 595 (2011).
[3] M. Turkyilmazoglu, Chem. Eng. Sci. **84**, 182 (2012).
[4] M. Turkyilmazoglu, Int. J. Mech. Sci. **53**, 886 (2011).
[5] M. Turkyilmazoglu, Int. J. Therm. Sci. **50**, 2264 (2011).
[6] T. Hayat, M. Awais, and S. Obaidat, Commun. Nonlinear Sci. Numer. Simulat. **17**, 699 (2012).
[7] S. Nadeem, A. Hussain, and M. Khan, Z. Naturforsch. **65a**, 540 (2010).
[8] N. S. Akbar, S. Nadeem, and C. Lee, Results Phys. **3**, 152 (2013).
[9] N. Santhosh, G. Radhakrishnamacharya, and A. J. Chamkha, J. Porous Media **18**, 71 (2015).
[10] S. Nadeem, B. Tahir, F. Labropulu, and N. S. Akbar, J. Aerospace Eng. **27**, 636 (2014).
[11] M. Farooq, N. Gulla, A. Alsaedia, and T. Hayat, J. Mech. **31**, 319 (2015).
[12] T. Hayat, S. Asad, and A. Alsaedi, Chinese Phys. B **24**, 044702 (2015).
[13] M. H. Abolbashari, N. Freidoonimehr, F. Nazari, and M. M. Rashidi, Powder Technol. **267**, 256 (2014).
[14] M. M. Rashidi, B. Rostami, N. Freidoonimehr, and S. Abbasbandy, Ain Shams Eng. J. **5**, 901 (2014).

[15] M. M. Rashidi, N. V. Ganesh, A. K. Abdul Hakeem, and B. Ganga, J. Mol. Liquids, **198**, 234 (2014).
[16] M. Turkyilmazoglu, Int. J. Heat Mass Transfer **57**, 82 (2013).
[17] S. Nadeem and S. Akram, Z. Naturforsch. **65a**, 483 (2010).
[18] A. Riaz, S. Nadeem, R. Ellahia, and A. Zeeshana, Appl. Bionics Biomech. **11**, 81 (2014).
[19] G. Ravikiran and G. Radhakrishnamacharya, J. Appl. Fluid Mech. **8**, 521 (2015).
[20] M. R. Hajmohammadi and S. S. Nourazar, Heat Transfer Eng. **35**, 863 (2014).
[21] R. Nazar, N. Amin, D. Filip, and I. Pop, Int. J. Nonlinear Mech. **39**, 1227 (2004).
[22] L. Crane, Z. angew. Math. Phys. **21**, 645 (1970).
[23] M. Mustafa, T. Hayat, I. Pop, S. Asghar, and S. Obaidat, Int. J. Heat Mass Transfer **54**, 5588 (2011).
[24] G. K. Ramesh, B. J. Gireesha, and C. S. Bagewadi, Int. J. Heat Mass Transfer **55**, 4900 (2012).